Research Article

Parity Violation and Magnetic Helicity on Cosmological Scales: From Turbulent Baryogenesis to Galaxy Clusters

Alexander Bershadskii[1]

1. ICAR, Israel

Using results of numerical simulations and the CMB data obtained by the Planck satellite mission, Atacama cosmology telescope, and Baryon Oscillation Spectroscopic Survey it is shown that chaotic/turbulent parity violation localized in long-lived magnetic blobs dominated by magnetic helicity takes place at cosmological lepto/baryogenesis. Analogous phenomenon has also been confirmed for magnetic fields in galaxy clusters. Despite the vast differences in the values of physical parameters and spatio-temporal scales between the numerical simulations and the cosmic observations, there is a quantitative agreement between the results of the cosmic observations and the numerical simulations in the frames of the distributed chaos notion.

Corresponding author: A. Bershadskii, bershads@gmail.com

I. Introduction

Baryogenesis at an earlier stage of the universe's development is one of the main candidates for magnetogenesis. The parity P (reflection symmetry) and charge-parity (CP) violation are a necessary part of the baryogenesis (Sakharov's conditions). Helical magnetic field emerges at these conditions. It should be noted that the electro-weak phase transition can also be involved in generating of helical magnetic field under these conditions (see, for instance, a review[1] and references therein).

The magnetic helicity can also be a key for solving the baryon asymmetry problem[2]. The lepto/baryogenesis epoch was rather turbulent because about all created baryons and antibaryons (as well as electrons and positrons) were annihilated, producing a huge amount of energy.

 doi.org/10.32388/PZ51AR.2

The point-wise (more precisely, the patch-like) helicity production is an inherent property of the 3D chaotic/turbulent motion of the plasmas/fluids. In such flows, the helicity appears spontaneously (even in the cases of zero net helicity) in pairs of patches having opposite signs of the helicity so that the net helicity remains zero. This phenomenon takes place in both non-magnetic (kinetic helicity) and magnetic (magnetic helicity) cases[3][4][5][6][7]. In the latter case, a part of the patches is transformed into long-lived magnetic blobs with sign-defined helicity and reduced dissipation[6][8]. Despite the net helicity is remaining zero the absolute value of the total normalized sum of the sign-defined helicities of the magnetic blobs $|I^{\pm}|$ ($I^{+} = -I^{-}$) can be used as a measure of spontaneous parity violation (see Section IV for more detail). In the present paper, we will study how this measure of parity violation is related to a measure of randomness of the chaotic/turbulent magnetic field (some other types of cosmological parity violation built on intrinsic reflection asymmetry of the particles one can find in a recent review[9] and therein).

The conception of smoothness can be used to quantify the levels of randomness of the chaotic/turbulent dynamical regimes. Indeed, the stretched exponential spectrum

$$E(k) \propto \exp -(k/k_{\beta})^{\beta} \tag{1}$$

is a characteristic feature of smooth chaotic dynamics. Here $1 \geq \beta > 0$ and k is the wavenumber.

The value of the $\beta = 1$ characterizes the deterministic chaos (see, for instance,[10][11][12][13][8] and references therein):

$$E(k) \propto \exp(-k/k_c). \tag{2}$$

When $1 > \beta$ the smooth chaotic dynamics can be already non-deterministic; this type of smooth dynamics can be called ‘distributed chaos’ (the term will be clarified below). Another term “soft turbulence” (suggested by[14]) can also be appropriate.

The parameter β could be used as an informative measure of randomization. Namely, the further the value of β is from $\beta = 1$ (which corresponds to the deterministic chaos), the more significant the system’s randomization. The smaller parameter β values are considered a precursor of hard turbulence[14].

For non-smooth dynamics (the hard turbulence[14]), the power-law (scaling) spectra are typical. This can happen, in particular, when the magnetic field can be considered as a passive field in a highly turbulent plasma[15].

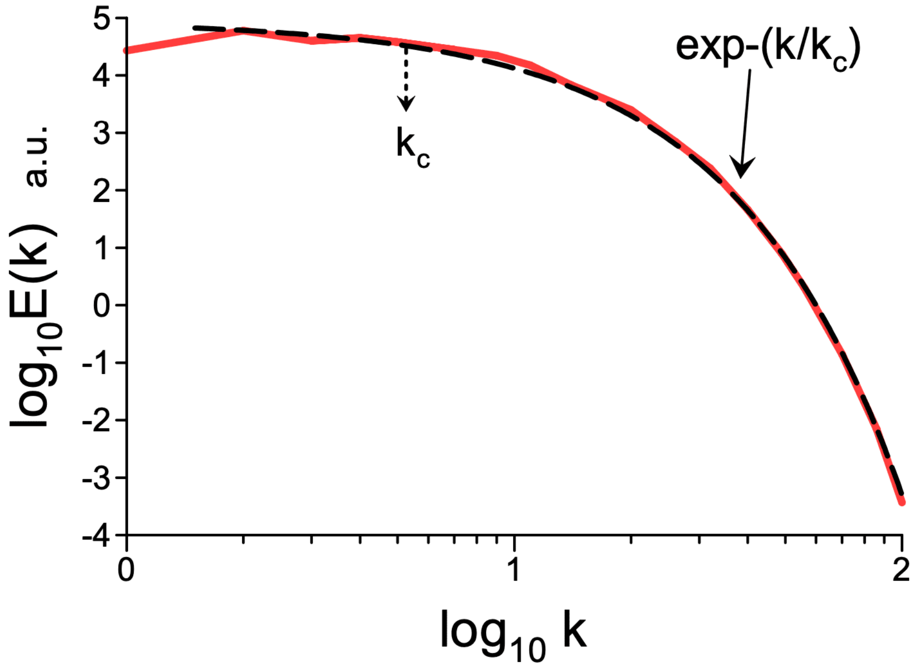

Figure 1. Magnetic energy spectrum at the saturated stage of fluctuating MHD dynamo for the Mach number $M \approx 0.11$ (numerical simulation).

Many models of baryogenesis were suggested, but there is a consensus to use the CMB data to estimate the present-day ratio of the number density of baryons (n_b) to photons (n_γ): $\eta_b = n_b/n_\gamma = 6.12 \times 10^{-10}$ [16]. This is the observational key for the baryogenesis problem (see, for a recent review, Ref.[17] and references therein). The extremely low observed value of the parameter η_b means, in particular, that the number of photons emitted by the recombination process itself is negligible in comparison with the number of photons that came from the previous epochs and were set free at the recombination epoch.

As was already mentioned above, most of the baryons B and antibaryons $\overline{B}$ were annihilated at the baryogenesis epoch, producing a vast amount of energy in the form of photons: $\gamma + \gamma \rightleftarrows B + \overline{B}$. Since these photons in the post-baryogenesis epoch had insufficient energy to turn into the baryon-antibarion pairs, most of them survived until the last scattering to become the CMB photons, that provides valuable information about the primordial matter-antimatter asymmetry (the η_b, in particular)[18]. Since the lepto/baryogenesis, magnetogenesis, the parity violation dominated by the magnetic helicity and the emission of the CMB-to-be photons are strongly interrelated one can expect that the level of the

doi.org/10.32388/PZ51AR.2

randomness of the magnetic field generated at the lepto/baryogenesis epoch could be imprinted on the level of randomness of the temperature of the CMB-to-be photons.

The continuing inflation smoothed out the strong fluctuations characterizing the lepto/baryogenesis epoch. At the recombination epoch, only tiny remnants of these fluctuations were present in the matter's motion and CMB. The remnants of the randomness, peculiar to the lepto/baryogenesis epoch's fluctuations, could also be preserved in the spatial power spectrum of the CMB temperature fluctuations (anisotropies) after the last scattering. Of course, this spectrum is a superposition of the remnant of the turbulent lepto/baryogenesis epoch, acoustic oscillations, etc. However, one can hope this remnant can be seen in the observed CMB spectrum and provide some information about the physical process at the lepto/baryogenesis epoch (see also an interesting discussion of present attempts to approach the problem in a recent paper[19] and references therein).

The observational estimates of the magnetic fields of the galaxy clusters turned out to be much larger than those predicted for the primordial magnetic fields. Therefore, different mechanisms of amplification of the seed magnetic fields (which supposedly came from the primordial stage) by the intensive (chaotic/turbulent) motion of the electrically conducting galaxy cluster plasmas were suggested in the literature. In the galaxy clusters, the chaotic/turbulent motion could be generated by cluster mergers, structure formation shocks, active galactic nuclei outflows, and the moving galaxy wakes.

Numerous models (numerical simulations) of the galaxy clusters magnetohydrodynamic dynamo were suggested (see, for instance,[20][21][22] and references therein). Some recent models will be discussed below in detail.

There are certain hints of a parity violation in the magnetized intracluster plasmas. However, it is not clear whether the magnetic helicity in this case has a primordial origin or generated by the turbulent motion of the intracluster plasmas. Till now, technically, all observables related to the galaxy clusters' magnetic fields are entangled and mixed with other physical characteristics of the magnetized plasmas (electron density, for instance). The observable Faraday rotation maps were used to infer information about the intracluster magnetic field (see, for instance, [23]). It will be shown below that the chaotic/turbulent magnetic field with the parity violation imprints its level of randomness on the Faraday rotation measure (cf the situation with the CMB above).

II. Deterministic Chaos in Magnetized Plasma

In a recent paper[24] a numerical simulation of a small-scale (fluctuating) dynamo with parameters favorable to deterministic chaos was performed using magnetohydrodynamic (MHD) equations

$$\frac{\partial \rho}{\partial t} + \nabla \cdot (\rho \mathbf{u}) = 0, \tag{3}$$

$$\frac{\partial \mathbf{b}}{\partial t} = \nabla \times (\mathbf{u} \times \mathbf{b}) + \eta \nabla^2 \mathbf{b}, \tag{4}$$

$$\frac{\partial \mathbf{u}}{\partial t} + (\mathbf{u} \cdot \nabla)\mathbf{u} = -\frac{\nabla p}{\rho} + \frac{\mathbf{j} \times \mathbf{b}}{c\rho} + \nu \left(\nabla^2 \mathbf{u} + \frac{1}{3} \nabla (\nabla \cdot \mathbf{u}) + 2\mathbf{S} \cdot \nabla \ln \rho \right) + \mathbf{F}, \tag{5}$$

in a triply-periodic cubic domain. In these equations $\mathbf{u}$ is the plasma velocity field, $\mathbf{b}$ is the divergence-free magnetic field, ρ is the plasma density, p is the plasma pressure, ν is the plasma viscosity, η is the plasma magnetic diffusivity, $\mathbf{j} = (c/4\pi)\nabla \times \mathbf{b}$ was taken for electric current density, c is the speed of light, $S_{ij} = \frac{1}{2}(u_{i,j} + u_{j,i} - \frac{2}{3}\delta_{ij}\nabla \cdot \mathbf{u})$ was taken for the rate-of-strain tensor, and $\mathbf{F}$ is a random delta-correlated in time solenoidal forcing function. An isothermal equation of state, $p = c_s^2 \rho$, was assumed with constant sound speed c_s.

The Reynolds and magnetic Reynolds numbers $\mathrm{Re} = \mathrm{Re}_m = 1122$, the Mach number $M \approx 0.11$, and the magnetic Prandtl number $\mathrm{Pr}_m = 1$. A weak random magnetic field (with zero net flux across the computational domain) was used as an initial seed field.

Figure 1 shows the one-dimensional (shell-averaged) magnetic energy spectrum at the saturated stage of the dynamo (the spectral data were taken from Figure 2 of the paper[24]). The dashed curve is the best fit corresponding to Eq. (2) (deterministic chaos).

III. Distributed Chaos Dominated by Magnetic Helicity

The ideal MHD has three fundamental quadratic invariants: total energy, cross and magnetic helicity[25]. The validity of magnetic helicity conservation increases with the magnetic Reynolds number value Re_m.

The average magnetic helicity density is

$$h_m = \langle \mathbf{a} \cdot \mathbf{b} \rangle \tag{6}$$

here $\mathbf{a}$ is the vector potential, $\mathbf{b} = [\nabla \times \mathbf{a}]$ is the fluctuating magnetic field, and $\langle \ldots \rangle$ means spatial average (for the fluctuating variables $\langle \mathbf{a} \rangle = \langle \mathbf{b} \rangle = 0$).

The magnetic helicity can be considered as an adiabatic invariant not only in the ideal MHD but also in a weakly dissipative magnetized plasma (see for instance,[26]), that makes it especially interesting for real astrophysical plasmas.

The transition from deterministic chaos to a distributed one can be considered as a randomization. Namely, the change of physical parameters can result in the random fluctuations of the characteristic scale k_c in equation (2). One has to take this phenomenon into account. It can be done using an ensemble averaging

$$E(k) \propto \int_0^\infty \mathcal{P}(k_c) \exp -(k/k_c) dk_c \tag{7}$$

Here, a probability *distribution* $\mathcal{P}(k_c)$ describes the random fluctuations of k_c. This is the rationale behind the name 'distributed chaos'.

For the magnetic field dynamics dominated by the magnetic helicity the scaling relationship between characteristic values of k_c and B_c based on dimensional considerations

$$B_c \propto |h_m|^{1/2} k_c^{1/2} \tag{8}$$

can be used to find the probability distribution $\mathcal{P}(k_c)$.

The value of B_c can be taken half-normally distributed $\mathcal{P}(B_c) \propto \exp -(B_c^2/2\sigma^2)$ ([27]). It is a normal distribution with a zero mean, which is truncated to have a nonzero probability density function for positive values of its argument only. For instance, if B is a normally distributed random variable, then the variable $B_c = |B|$ is half-normally distributed ([28]).

From Eq. (8) we then obtain

$$\mathcal{P}(k_c) \propto k_c^{-1/2} \exp -(k_c/4k_\beta) \tag{9}$$

It is the chi-squared probability distribution where k_β is a new constant).

Substituting Eq. (9) into Eq. (7) one obtains

$$E(k) \propto \exp -(k/k_\beta)^{1/2} \tag{10}$$

IV. Spontaneous Breaking of Local Reflection Symmetry

For chaotic/turbulent flows with global reflection symmetry the net magnetic helicity is equal to zero, whereas the point-wise magnetic helicity is not (because of the spontaneous breaking of the local reflection symmetry, see Introduction). The spontaneous local symmetry breaking in such flows is accompanied by the emergence of the blobs with non-zero magnetic helicity[25][8][29][6]. The magnetic surfaces of these blobs can be defined by the boundary conditions: $\mathbf{b}_n \cdot \mathbf{n} = 0$, where $\mathbf{n}$ is a unit vector normal to the boundary of the blob. The magnetic helicity (and its adiabatic conservation) suppresses energy dissipation in such blobs considerably[29], that results in the long-term survival of these blobs in chaotic/turbulent environments.

The sign-defined magnetic helicity of the j-blob can be defined as

$$H_j^{\pm} = \int_{V_j} (\mathbf{a}(\mathbf{x},t) \cdot \mathbf{b}(\mathbf{x},t)) d\mathbf{x} \tag{11}$$

where ('+' or '-') denotes the blob's helicity sign. The $H_j^{\pm}$ is an adiabatic invariant[25].

Then we can consider the total sign-defined adiabatic invariant

$$I^{\pm} = \lim_{V \to \infty} \frac{1}{V} \sum_j H_j^{\pm} \tag{12}$$

The summation takes into account the blobs with a certain sign only ('+' or '-'), and V is the total volume.

The adiabatic invariant $I^{\pm}$ defined by Eq. (12) can be used instead of the averaged magnetic helicity density h_m in the above estimate Eq. (8) for the special case of the local reflection symmetry breaking

$$B_c \propto |I^{\pm}|^{1/2} k_c^{1/2} \tag{13}$$

and the spectrum Eq. (10) can be also obtained for this case.

In recent papers[30][31] numerical simulations similar to that considered in Section II were performed (the net magnetic helicity was also negligible), but in these simulations the large Mach number $M = 10$ was achieved. Figure 2 shows the magnetic energy spectra computed in these numerical simulations. The spectral data shown in this figure were taken from Figure C4 of the Ref.[31]. While for the small Mach number $M = 0.1$ the bottom dashed curve in Figure 2 indicates the exponential spectrum Eq. (2) (deterministic chaos, cf Figure 1), for the large Mach number $M = 10$ the top dashed curve indicates a stretched exponential spectrum Eq. (10) with $\beta = 1/2$. This indicates the distributed chaos dominated by magnetic helicity, i.e. the spontaneous breaking of local reflection symmetry.

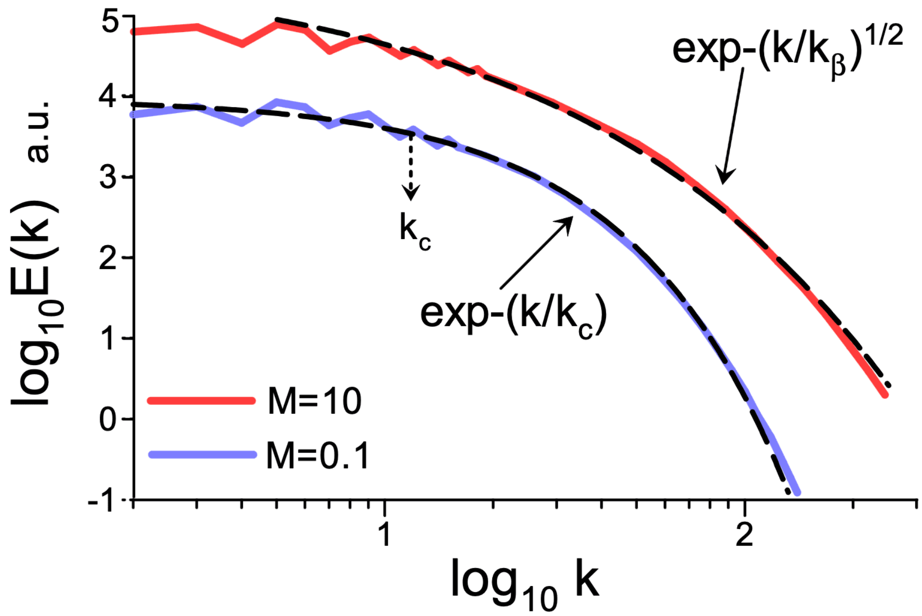

Figure 2. Magnetic energy spectra at the saturated stage of the fluctuating MHD dynamo for the Mach numbers $M = 0.1$ (bottom) and $M = 10$ (top). Numerical simulations.

In a recent paper[32] numerical simulations of magnetized ultrarelativistic plasma in an expanding flat universe at the radiation-dominated epoch after the electro-weak phase transition were performed using the comoving equations

$$\frac{\partial \ln \rho}{\partial t} = -\frac{4}{3}(\nabla \cdot \mathbf{u} + \mathbf{u} \cdot \nabla \ln \rho) + \frac{1}{\rho}\left[\mathbf{u} \cdot (\mathbf{J} \times \mathbf{B}) + \eta \mathbf{J}^2\right], \tag{14}$$

$$\begin{aligned}\frac{\partial \mathbf{u}}{\partial t} &= -\mathbf{u} \cdot \nabla \mathbf{u} + \frac{\mathbf{u}}{3}(\nabla \cdot \mathbf{u} + \mathbf{u} \cdot \nabla \ln \rho) + \frac{2}{\rho}\nabla \cdot (\rho \nu \mathbf{S}) \\ &\quad - \frac{1}{4}\nabla \ln \rho - \frac{\mathbf{u}}{\rho}\left[\mathbf{u} \cdot (\mathbf{J} \times \mathbf{B}) + \eta \mathbf{J}^2\right] + \frac{3}{4\rho}\mathbf{J} \times \mathbf{B},\end{aligned} \tag{15}$$

$$\frac{\partial \mathbf{B}}{\partial t} = \nabla \times (\mathbf{u} \times \mathbf{B} - \eta \mathbf{J} + \mathbf{F}). \tag{16}$$

The random electromotive force $\mathbf{F}$ simulates the generation of magnetic fields and was activated for a short duration (10% of the Hubble time). Two forcing cases were considered: fully helical and with negligible helicity. The simulations were performed in a periodic cubic box. The magnetic Pandtl number $Pr_m = \nu/\eta = 1$.

doi.org/10.32388/PZ51AR.2

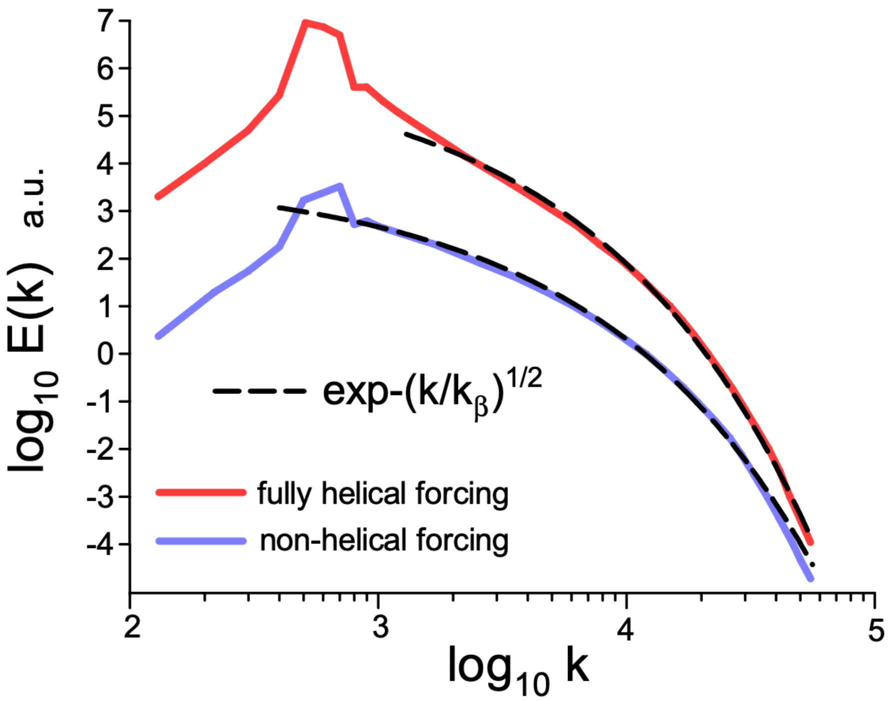

Figure 3. Magnetic energy spectra in an expanding flat universe at the radiation-dominated epoch after the electro-weak phase transition (numerical simulations). The spectra are vertically shifted for clarity.

 doi.org/10.32388/PZ51AR.2

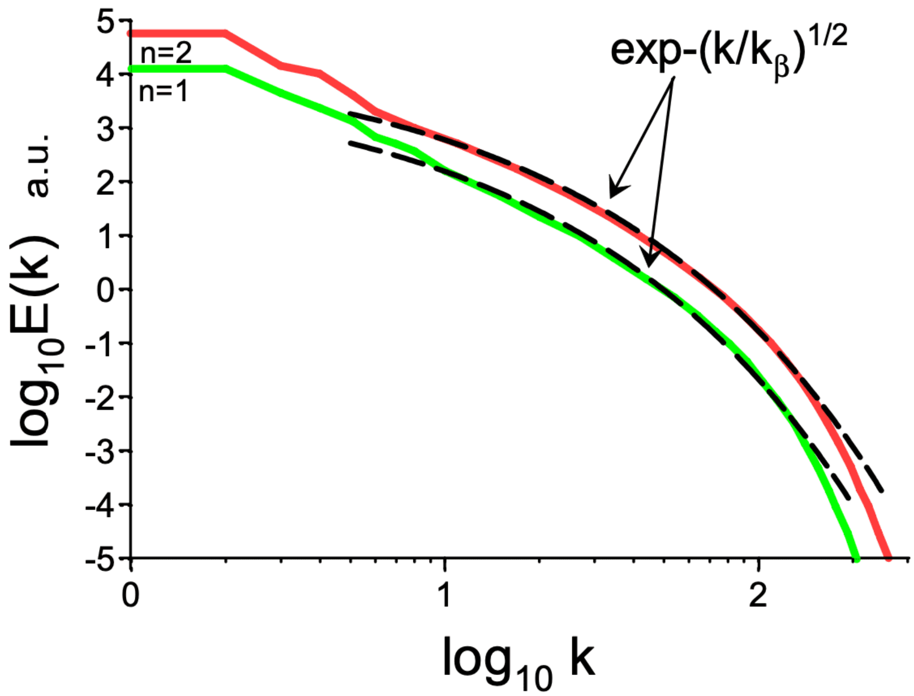

Figure 4. Magnetic energy spectra in relativistic fermions' plasmas generated due to a nonzero chiral chemical potential fluctuations μ_5 (numerical simulations). The spectra are vertically shifted for clarity.

The magnetic energy spectra shown in Figure 3 were computed at the time when the magnetic energy density reached its maximum. The spectral data were taken from Figures 2 and 3 of the Ref.[32]. The dashed curves indicate the magnetic helicity-dominated spectrum Eq. (10) for both cases: with fully helical (top) and non-helical (bottom) forcing. In the latter case, one can recognize the spontaneous parity violation caused by the chaotic/turbulent dynamics of the magnetized primordial plasma.

The above-discussed macroscopic mechanism of the chaotic/turbulent parity breaking and magnetic helicity generation can also boost the microscopic mechanisms of the parity breaking and magnetic helicity generation. Let us consider an example.

In a recent paper[33], the generation of the large-scale magnetic field in relativistic fermion's plasmas due to a nonzero chiral chemical potential fluctuations μ_5 (at initial $\langle \mu_5 \rangle = 0$) were studied using direct numerical simulation. The nonzero chiral potential appears in spatial areas of plasma where the chemical potentials of right and left-handed fermions are different. The chiral magnetohydrodynamic equations were used for this purpose

$$\frac{\partial \mathbf{B}}{\partial t} = \nabla \times [\mathbf{u} \times \mathbf{B} - \eta(\nabla \times \mathbf{B} - \mu_5 \mathbf{B})], \tag{17}$$

$$\rho \frac{D\mathbf{u}}{Dt} = (\nabla \times \mathbf{B}) \times \mathbf{B} - \nabla p + \nabla \cdot (2\nu\rho \mathbf{S}), \tag{18}$$

$$\frac{D\rho}{Dt} = -\rho \nabla \cdot \mathbf{u}, \tag{19}$$

$$\frac{D\mu_5}{Dt} = \mathcal{D}_5(\mu_5) + \lambda\eta[\mathbf{B} \cdot (\nabla \times \mathbf{B}) - \mu_5 \mathbf{B}^2], \tag{20}$$

where λ is the chiral feedback parameter, the hyperdiffusion operator $\mathcal{D}_5(\mu_5) = -\mathcal{D}_5 \nabla^4 \mu_5$. Unlike the standard MHD, here one can speak about the conservation of total chirality $\langle \mathbf{A} \cdot \mathbf{B} \rangle + 2\langle \mu_5 \rangle / \lambda$ (for $\langle \mu_5 \rangle = 0$ it is the magnetic helicity). The isothermal equation of state $p = \rho c_s^2$ relates pressure and density.

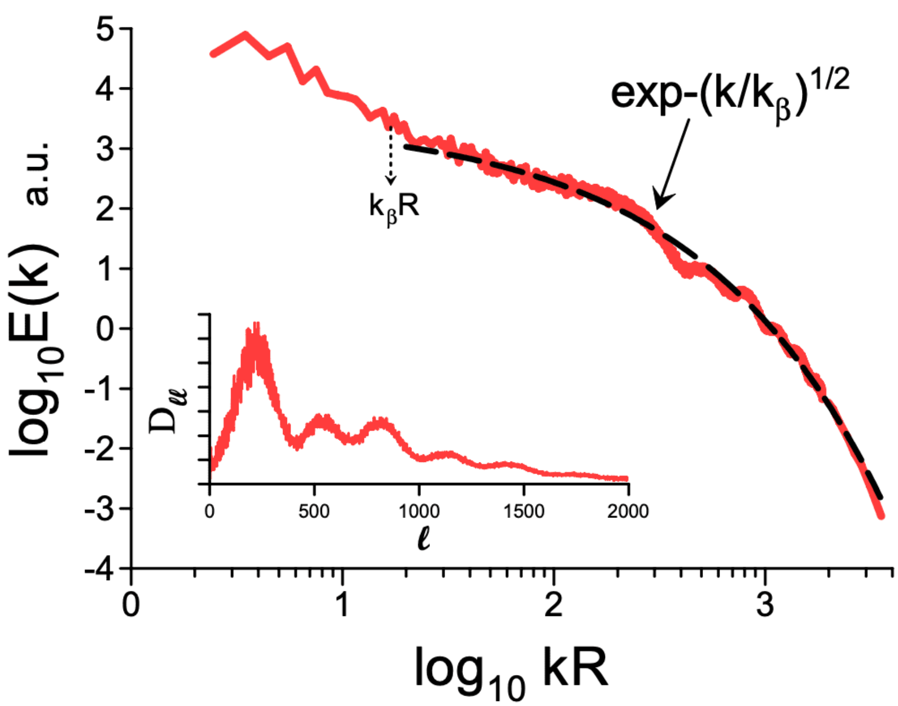

Figure 5. Power spectrum of CMB temperature fluctuations: Planck + ACT measurements. The insert shows the same spectral data (Planck) in the form $D_{ll} = l(l+1)C_l$ vs l in the linear-linear scales, usually used to emphasize the baryon acoustic peaks (at the large values $l \approx kR$).

doi.org/10.32388/PZ51AR.2

The equations were numerically solved in a periodic spatial box. Initial fluctuations of the chiral chemical potential μ_5 were taken as a Gaussian noise with spectrum $E_5(t_0) \propto k^{-n} \exp(-k^2/k_{cut}^2)$. The initial $\langle \mu_5 \rangle = 0$, and the initial magnetic helicity was negligible. The initial velocity field was absent, whereas initial (seed) magnetic field fluctuations were small. The dynamo was activated on small spatial scales due to the initial fluctuations of the chiral chemical potential, the Lorentz forces generated the magnetically dominated chaotic/turbulent plasma motion, and the inverse cascade (related to the magnetic helicity conservation) supposedly produced the large-scale magnetic field.

We will consider the runs performed with $n = 1, 2$. Figure 4 shows the magnetic energy spectra computed when the peak of the dynamo magnetic energy had the size of the computational box. The spectral data for Figure 4 were taken from Figure 4 of the Ref.[33].

The dashed curves indicate correspondence to the stretched exponential Eq. (10).

V. Signature of the Parity Violation at the Lepto-Baryogenesis Epoch in the CMB Spectrum

Figure 5 shows a combined (Planck+ACT) power spectrum of CMB temperature fluctuations obtained by the Planck mission and Atacama Cosmology Telescope (ACT). The CMB data shown in Figure 5 were cleaned from the foreground by the Planck and ACT teams. The spectral data were taken from the corresponding sites[34][35]. The ACT data were used for $kR > 1900$.

At the Planck and ACT sites the spectral data are given for the angular power spectra C_l vs the spherical multipole (or spherical harmonic degree) l. Using a 2D plane wavevector approximation[36] the spherical multipole l can be related to a wavenumber $k_l = \sqrt{l(l+1)}/R$, where R is the sphere's radius, and the azimuthally averaged 2D power spectral density $E(k_l) \approx R^2 C_l/\pi$[36].

The dashed curve indicates correspondence to the stretched exponential spectrum Eq. (10) (the vertical dotted arrow indicates position of $k_\beta R$). With the assumption that the magnetic field at the lepto/baryogenesis epoch imprints its level of randomization on the temperature of the CMB–to–be photons (see Introduction), Figure 5 can be considered as an indication that the remnant spectrum from the lepto/baryogenesis epoch can indeed be seen in the CMB spectrum.

The waviness of the spectrum can be related to the baryon acoustic oscillations as one can see from the insert in Figure 5, where the same spectral data (Planck) has been shown in the form $D_{ll} = l(l+1)C_l$ vs

l in the linear-linear scales. This presentation is usually used to emphasize the baryon acoustic peaks (at the large values $l \approx kR$).

The randomization with $\beta = 1/2$ provides evidence of the parity violation and the magnetic helicity domination over the emission of the CMB-to-be photons at the lepto/baryogenesis epoch (at least for the middle and small scales).

VI. Signature of the Parity Violation at the Lepto-Baryogenesis Epoch in the Baryon Oscillation Spectroscopic Survey

The processes in the epochs preceding the recombination imprinted themselves not only on the radiation but also on the surviving baryons, which were tightly coupled with the photons. The baryon acoustic oscillations -BAO (which caused the waviness of the CMB spectrum in Figure 5) were imprinted on the baryon matter distribution, which can now be observed in the sky. The traces of the BAO in the clustering of galaxies can be used as a ruler in measuring the distance–redshift relations. This method was employed for constructing the famous Baryon Oscillation Spectroscopic Survey - BOSS, mapping the spatial distribution of luminous red galaxies and quasars[37][38]. Figure 6 (adapted from the site[39], courtesy of C. Blake and S. Moorfield) shows a sketch illustrating the idea.

doi.org/10.32388/PZ51AR.2

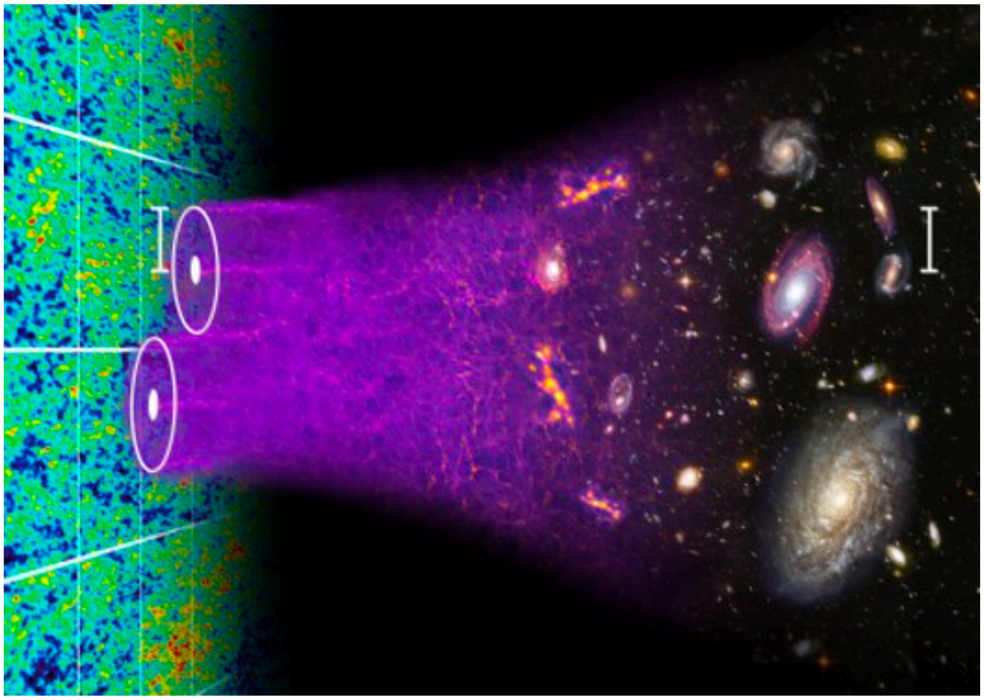

Figure 6. Sketch illustrating the idea of imprinting the primordial baryon spatial distribution on the baryon matter distribution, which can now be observed in the sky (courtesy of C. Blake and S. Moorfield).

The power spectrum of a distribution of points (galaxies for a galactic sample) can be defined as the Fourier transform of the two-point correlation function:

$$P(\mathbf{k}) = \frac{n}{(2\pi)^{3/2}} \int \xi(\mathbf{r}) e^{i\mathbf{kr}} d^3\mathbf{r} \tag{21}$$

where n is the mean density. It seems simple but it is very difficult to calculate the real-space matter spectrum from a 3D galaxy survey due to survey geometry effects, effects of light-to-mass bias, redshift-space distortions, and many other practical complications.

doi.org/10.32388/PZ51AR.2

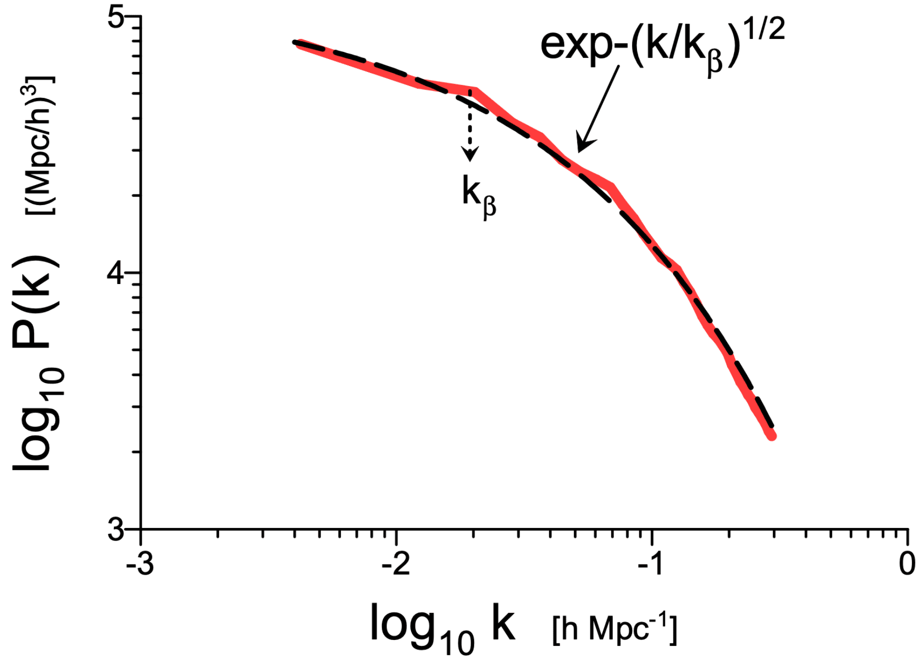

Figure 7. Power spectrum of baryon matter distribution computed for the Baryon Oscillation Spectroscopic Survey.

Figure 7 shows an isotropic $P(k)$ spectrum calculated using the data of the Baryon Oscillation Spectroscopic Survey (containing about one million galaxies). The spectral data were taken from the site[37] (see also Ref.[38]). The DR11 sample of the BOSS covers 8500 square degrees at the redshift range $0.2 < z < 0.7$.

The dashed curve in Figure 7 indicates the best fit by Eq. (10).

VII. Magnetic Field in Galaxy Clusters and Faraday Rotation Maps

A. Numerical simulations

The numerical models (simulations) not only allow a better understanding of the relevant physical processes but they become indispensable because of a principal difficulty of measurements (observations) of galaxy clusters' magnetic fields. Till now, technically, all observables related to the galaxy clusters' magnetic fields are entangled and mixed with other physical characteristics of the magnetized plasmas (electron density, for instance).

 doi.org/10.32388/PZ51AR.2

In a paper[40] spectra of the magnetic energy and corresponding spectra of the Faraday rotational measure maps were computed in the framework of the standard (collisional) magnetohydrodynamics and in the framework of a collisionless MHD model (which is expected to be more appropriate to the magnetized and weakly collisional intracluster plasma). This model is based on the dynamic equations

$$\frac{\partial \rho}{\partial t} + \nabla \cdot (\rho \mathbf{u}) = 0, \tag{22}$$

$$\frac{\partial (\rho \mathbf{u})}{\partial t} + \nabla \cdot \left[\rho \mathbf{u}\mathbf{u} + \left(\mathbf{P} + \frac{B^2}{8\pi} \right) \mathbf{I} - \frac{\mathbf{B}\mathbf{B}}{4\pi} \right] = \mathbf{f}, \tag{23}$$

$$\frac{\partial \mathbf{B}}{\partial t} - \nabla \times (\mathbf{u} \times \mathbf{B}) = 0, \tag{24}$$

where the pressure tensor is

$$\mathbf{P} = p_\perp \mathbf{I} + \left(p_\parallel - p_\perp \right) \hat{\mathbf{b}}\hat{\mathbf{b}}, \tag{25}$$

here $p_\perp = c_\perp^2 \rho$, $p_\parallel = c_\parallel^2 \rho$, $\hat{\mathbf{b}} = \mathbf{B}/|\mathbf{B}|$, and $c_\perp$ and $c_\parallel$ are the sound speeds perpendicular and parallel to the magnetic field $\mathbf{B}$, correspondingly.

The paper's authors[40] reported some indications of a small-scale (fluctuation) dynamo in work for their models.

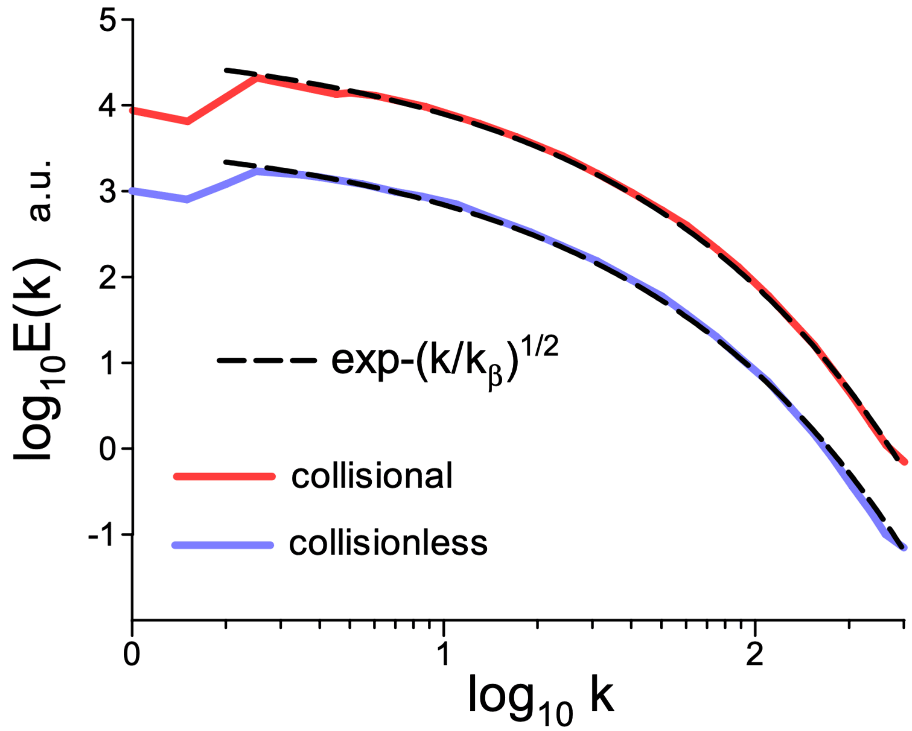

Figure 8. Magnetic energy spectra computed for the collisional (top) and collisionless (bottom) magnetohydrodynamics. The spectra are vertically shifted for clarity.

doi.org/10.32388/PZ51AR.2

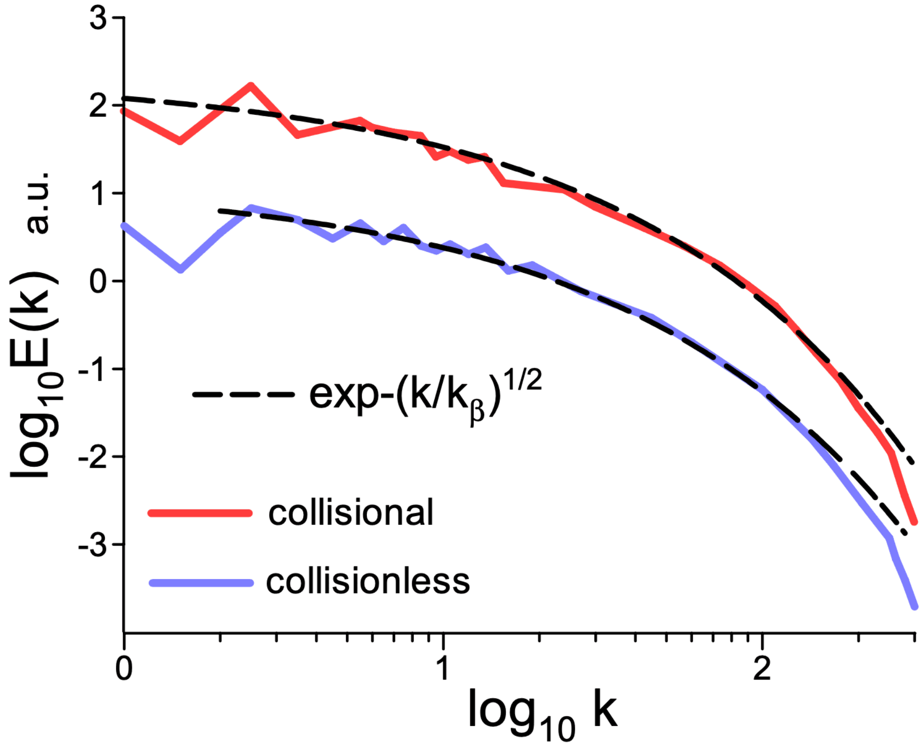

Figure 9. Power spectra of the Faraday rotational measure maps computed for the collisional (top) and collisionless (bottom) magnetohydrodynamics. The spectra are vertically shifted for clarity.

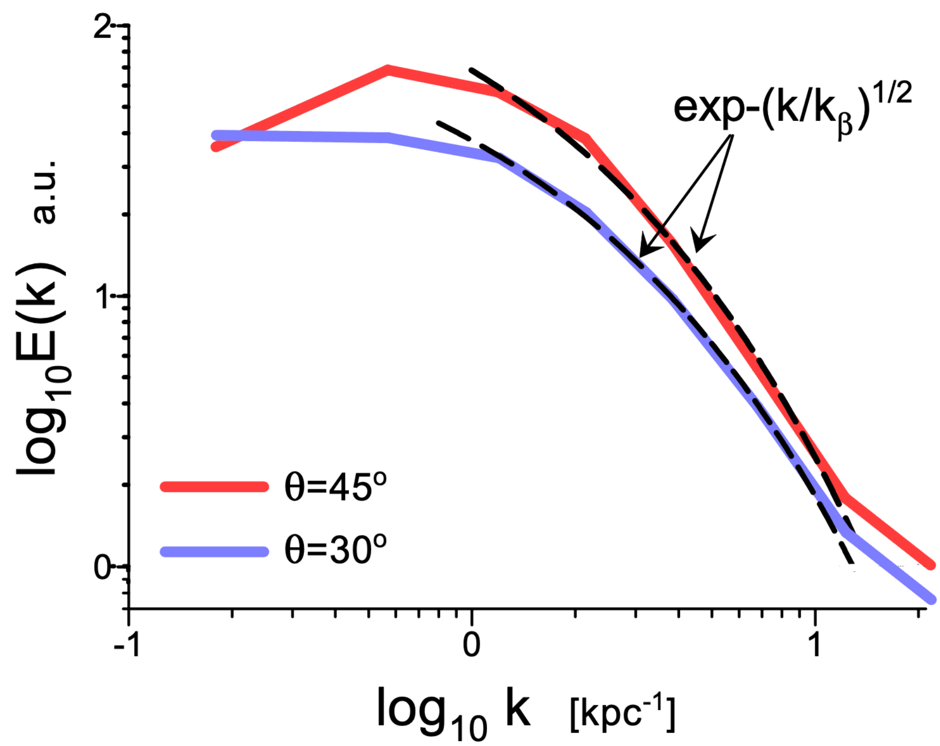

Figure 10. Intracluster magnetic power spectra for the northern radio lobe of Hydra A for two values of the inclination angles (between the line of sight and the northern lobe) $\theta = 45^o$ (top) and $\theta = 30^o$ (bottom).

Figure 8 shows the spectra of magnetic energy computed for the collisional (top) and collisionless (bottom) magnetohydrodynamics with a weak uniform external magnetic field $B_{ext} = 0.1$ and sound speed $c_{snd} = 0.1$ for collisional and $c_{\|} = 0.1$, $c_{\perp} = 0.05$ for collisionless cases (in terms of Ref.[40]). The spectral data were taken from Figures 6a and 6b of the paper[40]. The dashed curves indicate the best fit by the stretched exponential Eq. (10).

One can see that for both models interpretation of the spectral data for magnetic energy using the notion of the distributed chaos dominated by magnetic helicity Eq. (10) is in good agreement with the results of the numerical simulations.

Figure 9 shows the power spectra of the Faraday rotational measure maps corresponding to Figure 8. The spectral data were taken from Figures 12a,c of the paper[40]. The dashed curves indicate the best fit by the stretched exponential Eq. (10).

One can see that the magnetic field imprints its level of randomization on the Faraday maps. Therefore, the observational Faraday rotation measure maps could be used to obtain this information about the magnetic fields.

B. Observations

In a paper[23] the Faraday rotation maps of the northern radio lobe of Hydra A (a cool core galaxy cluster) were analyzed with a Bayesian maximum likelihood analysis to infer the intracluster magnetic field power spectrum. Figure 10 shows the magnetic power spectra for two values of the inclination angles (between the line of sight and the northern lobe) $\theta = 45^o$ (top) and $\theta = 30^o$ (bottom). The spectral data were taken from Figure 7 of the paper[23].

The dashed curve indicates the best fit by the stretched exponential Eq. (10) (cf previous section).

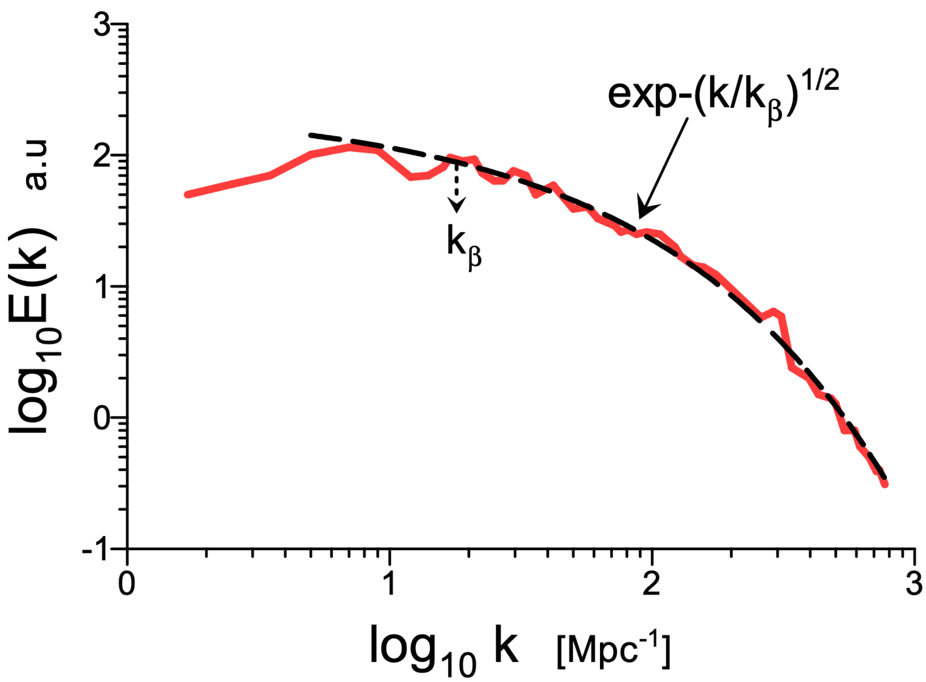

Figure 11. Radially averaged power spectrum of a Faraday rotation measure map for the galaxy cluster A119.

Figure 11 shows the radially averaged power spectrum of a Faraday rotation measure map for the galaxy cluster A119 (the spectral data were taken from Figure 10d of paper). This galaxy cluster is located in a region with a rather low Galactic rotation measure and consists of three extended radio galaxies. These galaxies are located at different projected distances (170, 453, and 1515 kpc) from the cluster center and the radio sources are highly polarized.

The dashed curve indicates the best fit by the stretched exponential Eq. (10).

VIII. Conclusions and Discussion

A parity violation mechanism related to the spontaneous appearance of sign-defined magnetic helicity in the long-lived magnetic blobes at turbulent lepto/baryogenesis has been suggested, and its traces in the CMB radiation (Planck and ACT measurements) and in the post-recombination baryonic matter distribution (BOSS observations) have been discussed.

Analogous mechanism related to the primordial seed magnetic field amplification in galaxy clusters and its traces in the Faraday rotation measure observations has also been suggested and discussed. The results of relevant numerical simulations have been used to support this approach.

The generalized (normalized) net magnetic helicity $I^{\pm}$ Eq. (12) has been used as a measure of the parity violation for the case of zero net magnetic helicity. The level of randomization (characterized by the parameter $\beta = 1/2$, see Introduction) of the primordial magnetic field has been related to the measure of parity violation $I^{\pm}$. Then, it has been argued that this level of randomization was imprinted on the CMB-to-be photons' temperature at the turbulent lepto/baryogenesis, and a remnant of this level of randomization remained in the CMB photons' temperature at the last scattering surface Figure 5.

The waviness in the CMB temperature spectrum can be be related to the primordial acoustic oscillations (insert in Figure 5). The idea that the baryon acoustic oscillations imprinted themselves on the observed baryonic matter distribution underlies the BOSS project (see Figure 6 and[38]). Therefore, one can expect that the level of randomization of the baryonic matter distribution observed by the BOSS will be the same $\beta = 1/2$ (see Figure 7).

An analogous situation takes place at the primordial seed magnetic field amplification in galaxy clusters, and its traces are found in the Faraday rotation measurement observations (see Figures 8-11).

Acknowledgements

I thank E. Levich, H.K. Moffatt, S. Mandal,, S. Pikovsky, and K.R. Sreenivasan for stimulating discussions. I also thank the Planck, ACT and BOSS teams for sharing their data.

References

1. ^K. Subramanian, The origin, evolution and signatures of primordial magnetic fields, Rep. Prog. Phys. 79, 0 7690 (2016).
2. ^K. Kamada, Return of grand unified theory baryogenesis: Source of helical hypermagnetic fields for the ba ryon asymmetry of the universe, Phys. Rev. D 97, 103506 (2018).
3. ^R.M. Kerr, Helicity generation in 3D Euler and turbulence, in: Elementary Vortices and Coherent Structures, Proceedings of the IUTAM Symposium Kyoto, 2004, 1–8.
4. ^D.D Holm, R.M. Kerr, Transient vortex events in the initial value problem for turbulence, Phys. Rev. Lett. 88, 244501 (2002).
5. ^D.D Holm, R.M. Kerr, Helicity in the formation of turbulence, Physics of Fluids 19, 025101 (2007).
6. a, b, cH.K. Moffatt, Magnetostatic equilibria and analogous Euler flows of arbitrarily complex topology. Part 1. Fundamentals, J. Fluid Mech. 159, 359–378 (1985).
7. ^A.A. Schekochihin, MHD turbulence: a biased review. J. Plasma Phys. 88, 155880501 (2022).
8. a, b, cA. Bershadskii, Magneto-inertial range dominated by magnetic helicity in space plasmas. Fundament al Plasma Physics 11, 100066 (2024).
9. ^V.B. Semikoz, D.D. Sokoloff, Effects of P-Noninvariance, Particles, and Dynamos, in: Helicities in Geophysic s, Astrophysics and Beyond (Eds. K. Kuzanyan, N. Yokoi, M.K. Georgoulis, R. Stepanov) AGU, 2023.
10. ^J.E. Maggs, G.J. Morales, Generality of deterministic chaos, exponential spectra, and Lorentzian pulses in m agnetically confined plasmas, Phys. Rev. Lett. 107, (2011) 85003 (2011).
11. ^J.E. Maggs, G.J. Morales, Origin of Lorentzian pulses in deterministic chaos, Phys. Rev. E 86, (2012) 015401 (R) (2012).
12. ^J.E. Maggs, G.J. Morales, Exponential power spectra, deterministic chaos and Lorentzian pulses in plasma e dge dynamics, Plasma Phys. Control. Fusion 54, (2012) 124041(2012).
13. ^S. Khurshid, D.A. Donzis, K.R. Sreenivasan, Energy spectrum in the dissipation range, Phys. Rev. Fluids 3, 08 2601(R) (2018).
14. a, b, cZ.-Z. Wu, L.P. Kadanoff, A. Libchaber, M. Sano, Frequency power spectrum of temperature fluctuations i n free convection. Phys. Rev. Lett., 64, 2140-2143 (1990).
15. ^A. Bershadskii, and K. R. Sreenivasan, Intermittency and the passive nature of the magnitude of the magn etic field. Phys. Rev. Lett. 93, 064501 (2004).

doi.org/10.32388/PZ51AR.2

16. [^]N. Aghanim, et al., Planck 2018 results I. Overview and the cosmological legacy of Planck. A&A 641, A1 (2020).

17. [^]D. Bödeker and W. Buchmüller, Baryogenesis from the weak scale to the grand unification. Rev. Mod. Phys. 93, 035004 (2021).

18. [^]V. Bromm and A. Smith, Cosmic microwave background (CMB). Lecture Notes, Univ. of Texas, Austin, 2014. https://www.as.utexas.edu/astronomy/education/spring14/bromm/secure/notes_apr_17.pdf

19. [^]O.H.E. Philcox, Do the CMB Temperature Fluctuations Conserve Parity?, Phys. Rev. Lett. 31, 181001 (2023).

20. [^]A. Ruzmaikin, D. Sokoloff, A. Shukurov, The dynamo origin of magnetic fields in galaxy clusters, MNRAS 241, 1-14 (1989).

21. [^]F. Vazza, M. Brüggen, C. Gheller, P. Wang, On the amplification of magnetic fields in cosmic filaments and galaxy clusters, MNRAS 445, 3706–3722 (2014).

22. [^]K. Subramanian, From primordial seed magnetic fields to the galactic dynamo, Galaxies 7, 47 (2019).

23. [a, b, c]C. Vogt, T.A. Enßlin, A Bayesian view on Faraday rotation maps – Seeing the magnetic power spectra in galaxy clusters, A&A 434, 67-76 (2005).

24. [a, b]A. Seta, P.J., Bushby, A. Shukurov, T.S. Wood, Saturation mechanism of the fluctuation dynamo ${Pr_{m}} \geq 1$, Phys. Rev. Fluids 5, 043702 (2020).

25. [a, b, c]H.K. Moffatt, A. Tsinober, Helicity in laminar and turbulent flow, Annu. Rev. Fluid Mech. 24, 281–312 (1993).

26. [^]Y. Zenati, E.T. Vishniac, Conserving local magnetic helicity in numerical simulations, ApJ 948, 11 (2023). Monin and Yaglom [2007] A.S. Monin, A.M. Yaglom, Statistical Fluid Mechanics, Vol. II: Mechanics of Turbulence, Dover Pub. NY, 2007.

27. [^]N.L. Johnson, S. Kotz, S., N. Balakrishnan, Continuous Univariate Distributions, Vol. 1, Wiley NY, 1994.

28. [^]H.K Moffatt, The degree of knottedness of tangled vortex lines, J. Fluid Mech. 35, 117–129 (1969).

29. [a, b]A. Seta, C. Federrath, Magnetic fields in the Milky Way from pulsar observations: effect of the correlation between thermal electrons and magnetic fields, MNRAS 502, 2220–2237 (2021).

30. [^]A. Seta, C. Federrath, J.D Livingston, N.M. McClure-Griffiths, Rotation measure structure functions with higher-order stencils as a probe of small-scale magnetic fluctuations and its application to the Small and Large Magellanic Clouds, MNRAS 518, 919–944 (2023).

31. [a, b]A.R. Pol, S. Mandal, A. Brandenburg, T. Kahniashvili, Polarization of gravitational waves from helical MHD turbulent sources, JCAP 04, 019 (2022).

32. a, b*J. Schober, I. Rogachevskii, A. Brandenburg, Production of a chiral magnetic anomaly with emerging turbulence and mean-field dynamo action, Phys. Rev. Lett. 128, 065002 (2022).*

33. a, b*Available at the site https://pla.esac.esa.int/pla/#cosmology.*

34. ^*Available at the site https://lambda.gsfc.nasa.gov/product/ act/.*

35. ^*S. Maus, The geomagnetic power spectrum, Geophys. J. Int. 174, 135–142 (2008).*

36. a, b*Available at the site https://www.sdss3.org/dr11/Anderson-2013-CMASSDR11-power-spectrum-post-recon-1.dat.*

37. a, b*L. Anderson et al. The clustering of galaxies in the SDSS-III Baryon Oscillation Spectroscopic Survey: baryon acoustic oscillations in the Data Releases 10 and 11 Galaxy samples, MNRAS 441, 24–62 (2014).*

38. a, b, c*Available at the site https://www.sdss4.org/boss-3.*

39. ^*M.S. Nakwacki, G. Kowal, R. Santos-Lima, E.M. de Gouveia Dal Pino, D.A. Falceta-Gonçalves, Features of collisionless turbulence in the intracluster medium from simulated Faraday Rotation maps, MNRAS 455, 3702–3723 (2016).*

40. a, b, c, d, e*M. Murgia, F. Govoni, L. Feretti, G. Giovannini, D. Dallacasa, R. Fanti, G.B. Taylor, K. Dolag, Magnetic fields and Faraday rotation in clusters of galaxies, A&A 424, 429-446 (2004).*

Declarations

Funding: No specific funding was received for this work.

Potential competing interests: No potential competing interests to declare.